Proceedings of the 19th Lunar and Planetary Science Conference, pp. 137-145

High Alumina (HA) and Very High Potassium (VHK) Basalt Clasts from Apollo 14 Breccias, Part 1—Mineralogy and Petrology: Evidence of Crystallization from Evolving Magmas

C. R. Neal, L. A. Taylor, and A. D. Patchen

Department of Geological Sciences, University of Tennessee, Knoxville, TN 37996

The mineralogy and petrography of very high potassium (VHK) and high alumina (HA) basalts from the Apollo 14 site provide an insight into their magmatic evolution. Generally, their parageneses are similar, with olivine and chromite the early liquidus phases, followed by plagioclase and pyroxene, which crystallized together. Although late-stage ilmenite and FeNi metal occur in both VHK and HA samples, the VHKs also crystallize K-feldspar and Fa-rich olivine. Zoning of constituent minerals is similar for both basalt types, demonstrating that the parental magmas for both HA and VHK basalts became enriched in K, Na, Ca, Fe, and Ti and depleted in Mg and Al as crystallization proceeded. Enrichment of K in the VHK basalts is above that expected from normal fractional crystallization, witnessed by an interstitial K-rich residual melt (7-12 wt% K_2O), and requires an external input of K. This is consistent with the granite assimilation model proposed for VHK basalt on the basis of whole-rock chemistry. The mineralogy and petrography of HA basalt suggest petrogenesis by fractional crystallization alone; however, whole-rock chemistry necessitates the involvement of KREEP.

INTRODUCTION

The mineralogical and petrographic analysis of 29 new basalt clasts allows the evolution of crystallizing magma(s) from the Apollo 14 site to be traced. These "new" basalt samples were obtained from the "pull apart" efforts of breccias 14303, 14304, and 14321. The data presented here are the first part of a two-part presentation, the second contribution (*Neal et al.*, 1989) presenting whole rock chemistry and major- and trace-element modeling.

This study investigates the mineralogy and petrography of basaltic clasts from the Apollo 14 site. We examine 22 new HA and 7 new VHK basalt clasts by petrographic and electron microprobe analytical techniques. The classification into HA and VHK varieties is made on the basis of whole-rock compositions (see *Neal et al.*, 1989), or by mineralogy. Mineralogically, K-feldspar and K-rich residual glass are present in VHK basalts, but not in the HA variety. In our descriptions samples will be referred to by thin-section number, with the INAA numbers in brackets. This will allow easy comparison of the mineralogy and petrology with the whole rock geochemistry presented in the second part of this study (*Neal et al.*, 1989).

PETROGRAPHY

VHK Basalts

The seven new VHK basalt samples are from breccias 14303 and 14304. Visually estimated modal proportions for these VHK basalts are presented in Table 1a. Textural variations preclude the categorization of these samples into petrographic groups, but small (<0.1 mm), petrographically unidentifiable overgrowths on plagioclase are present in all samples. Each sample will be briefly discussed in order of ascending thin-section number.

14303,328(318). This is a coarse-grained, ophitic basalt with pyroxene (32 modal %) and plagioclase (37 modal %), reaching up to 1.5 mm (Fig. 1a). Olivine (10 modal %) occurs as corroded crystals in the cores of pyroxene, and also as discrete grains, with chromite (up to 0.5 mm and 4 modal %) and FeNi metal (0.1 mm and 6 modal %) inclusions. Interstitial ilmenite and clear glass occur (4 and 2 modal %, respectively), along with minor opaque, interstitial glass, and troilite.

14304,169(168). This sample has an overall inequigranular or granulated texture (Fig. 1b) and is similar to the 14303-type VHK basalts described by *Neal et al.* (1988a). Plagioclase composes 54 modal % of the rock. Large (≈1 mm) plagioclase phenocrysts contain minor (≈2 modal %) rounded pyroxene inclusions (<0.2 mm). Pyroxenes (35 modal %) are interstitial (up to 0.5 mm) with groundmass plagioclase (0.1-0.2 mm). No olivine is present. Interstitial FeNi metal (1 modal %) is the only opaque.

14304,177(176). This is a coarse-grained (grain size 1-2.5 mm) noritic basalt with an interlocking texture (Fig. 1c) of pyroxene and plagioclase (45 and 40 modal %, respectively). Some pyroxenes occasionally exhibit wormy exsolution textures (<0.1 mm). Abundant interstitial brown glass is present (10 modal %). Iron-nickel metal (<0.2 mm and 2 modal %)) is the only opaque mineral present. The thin-section chip is very small (2 × 4 mm) and the modal data may not be representative.

14304,187(148). This sample is a coarse-grained (grain size 1-1.5 mm) ophitic basalt similar to 14303,328(318) (Fig. 1a), dominated by pyroxene and plagioclase (38 and 34 modal %, respectively). Olivine (12 modal %) is present both as cores in pyroxenes (≈0.1-0.4 mm with FeNi metal inclusions) and as discrete grains (≈0.3 mm). Interstitial chromite (0.1-0.3 mm and 4 modal %) is the dominant opaque phase (also found as ≈0.1 mm inclusions in olivine), followed by

TABLE 1a. Visually estimated modal proportions for the VHK basalts.

	14303 ,328	14304 ,169	14304 ,177	14304 ,187	14304 ,189	14304 ,194	14304 ,203
Olivine	10	—	—	12	9	5	23
Pyroxene	32	35	45	38	36	30	22
Plagioclase	37	54	40	34	30	26	30
Orthoclase	3	4	3	5	4	6	2
Ilmenite	4	—	—	—	6	10	6
Chromite	4	—	—	4	5	5	5
FeNi Metal/ Troilite	6	1	2	2	8	8	5
Glass	2	6	10	5	2	10	5

FeNi metal and troilite (<0.1 mm). Clear and brown interstitial glass (5 modal %) is also present.

14304,189(152). This is a granulated basalt with a relict ophitic texture (grain size 1-1.5 mm). Pyroxenes and truncated plagioclase laths (36 and 30 modal %, respectively) form an interlocking network, with rare corroded olivines (≈0.2 mm and 9 modal %), but triple junctions are rare (Fig. 1d). Iron-nickel metal and chromite (both <0.05 mm) inclusions occur in olivine. Interstitial ilmenite (0.5 mm) is the dominant opaque phase (6 modal %), with rare interstitial FeNi metal and troilite (<0.1 mm). Small areas of interstitial brown glass (2 modal %) are present.

14304,194(164). This is a fine-grained quench-textured basalt (0.1-0.3 mm: Fig. 1e) with rounded and dendritic olivine (5 modal %), pyroxene prisms (30 modal %), plagioclase laths (26 modal %), and a high proportion of opaque glass (10 modal %). Much interstitial ilmenite, FeNi metal, and opaque glass (10, 5, and 10 modal %, respectively) exists. Minor interstitial troilite is also present.

14304,203(180). This is another fine-grained basalt, but with olivine phenocrysts up to 0.5 mm (containing ≈0.1 mm inclusions of chromite) and a smaller proportion of interstitial glass than in 14304,194(164) (5 modal %). Pyroxenes (22 modal %), smaller olivines, and plagioclase laths (30 modal %) form the groundmass (Fig. 1f). Olivine makes up approximately 23% of the specimen. Small ilmenites, FeNi metal, and troilite grains (0.1 mm) are associated with clear interstitial glass.

HA Basalts

The 22 new HA basalts are all from breccia 14321 and have been divided into three categories based on texture: (1) ophitic, (2) subophitic, and (3) inequigranular or granulated. Visually estimated modal proportions are given in Table 1b and numbers of samples forming these groups are given in Table 4.

Ophitic. Basalts exhibiting ophitic textures (Fig. 2a) are generally fine grained (0.1-1 mm), and all contain large (up to 1.5 mm) olivine phenocrysts (3-16 modal %) set in a network of 0.2-1 mm pyroxene (16-38 modal %) and plagioclase laths (18-35 modal %). Small (<0.1 mm) euhedral chromites (0-5 modal %) are usually present as inclusions in olivine. Most plagioclase laths overlay the pyroxene prisms, although they are not poikilitically enclosed. However, a small proportion of plagioclase laths are terminated by the pyroxene prisms. A few olivines have mantles of pyroxene, which vary in width from a small (<0.1 mm) rind to cases in which olivine forms a core to a pyroxene grain (up to 1.5 mm). Ilmenite, SiO_2, troilite, and FeNi metal (up to 0.2 mm, 0.1 mm, <0.1 mm, and <0.1 mm, respectively) form interstitial phases in these basalts (see Table 1b for modes). Residual opaque glass (2-20 modal %) is present.

Subophitic. Basalts of this textural subgroup (Fig. 2b) contain larger pyroxenes and plagioclase laths (35-52 and 20-40 modal %, respectively; both 1-2 mm) than does the ophitic group. The relationship between plagiocase and pyroxene described in the ophitic basalts occurs here also, but a greater proportion of plagioclase laths are terminated by pyroxene. Olivine (0-8 modal %) is present only in the cores of pyroxenes, or is absent. Subhedral to euhedral chromites (<0.1 mm and 0-5 modal %) are usually present and associated with pyroxene. Ilmenite, SiO_2 (up to 0.5 mm), troilite, and FeNi metal (<0.1 mm) are interstitial phases (see Table 1b for modes). Only minor interstitial glass is present in these basalts (0-6 modal %).

Inequigranular. Members of this textural subgroup exhibit either a partial or overall inequigranular or granulated texture (Fig. 2c). However, all basalts in this category also exhibit relict textures, either ophitic or subophitic, suggesting this textural group includes basalts from the previous two groups (see Table 1b for modes). Granulation of these basalts occurred without much recrystallization. As such, grain size and the relationship of the phases to each other are more varied than in the groups described above, but generally fall into either of the above categories.

TABLE 1b. Visually estimated modal proportions for the HA basalts.

	Granulated HA	Subophitic HA	Ophitic HA
Olivine	0-10	0-8	3-16
Pyroxene	25-45	35-52	16-38
Plagioclase	20-45	20-40	18-35
Ilmenite	6-12	10-16	5-15
Chromite	0-8	0-5	0-5
FeNi Metal/ Troilite	1-9	1-6	2-11
SiO_2	0-5	0-3	0-6
Glass	2-22	0-6	2-20

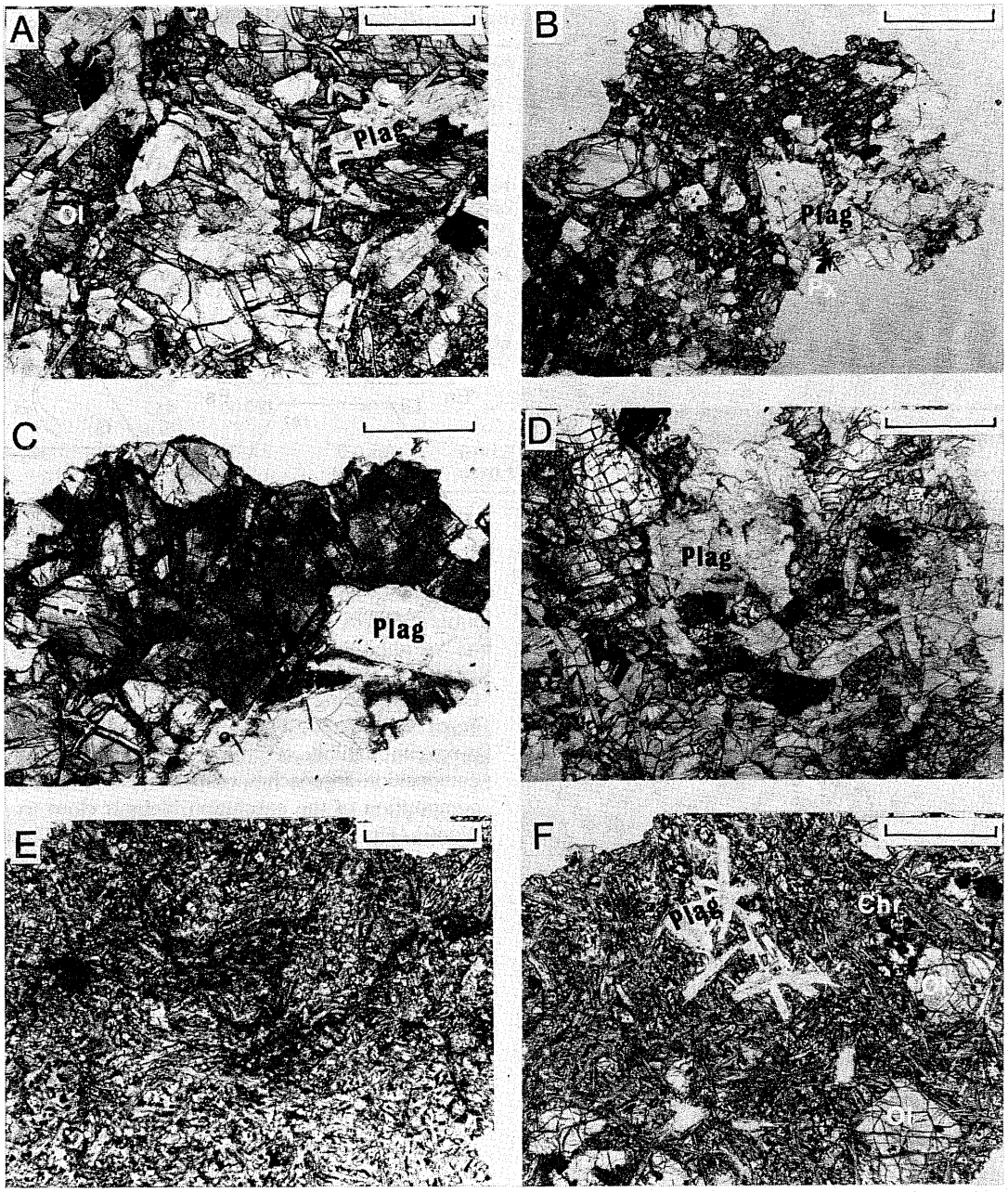

Fig. 1. Six photomicrographs demonstrating the range in VHK basalt textures. The scale bar represents 0.5 mm: **(a)** 14303,328, a coarse-grained ophitic basalt; **(b)** 14304,169, similar to the 14303-type described by *Neal et al.* (1988b); **(c)** 14304,177, a coarse grained noritic basalt; **(d)** 14304,189, a granular basalt with a relict subophitic texture; **(e)** 14304,194, a fine-grained, vitrophyric basalt; **(f)** 14304,203, a fine-grained, ophitic basalt with olivine phenocrysts.

MINERAL CHEMISTRY

The compositions of constituent minerals were determined using a CAMECA SX-50 electron microprobe at the University of Tennessee. Accelerating voltage was 15 kV with a filament current of 100 uA. Beam current used for all phases was 30 nA, except for feldspars and glasses when 20 nA was employed (beam current was measured by a Faraday cup); counting times were 20 sec. All data were corrected using ZAF procedures.

VHK Basalts

Pyroxene compositions from the VHK basalts are variable, ranging from enstatite and pigeonite (En60-66; Wo2-10) to augite and ferro-augite (Wo30-46; Fs21-39) (Table 2; Fig. 3).

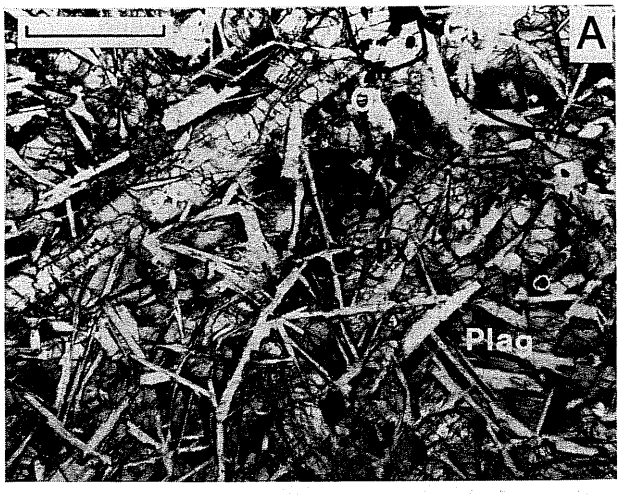

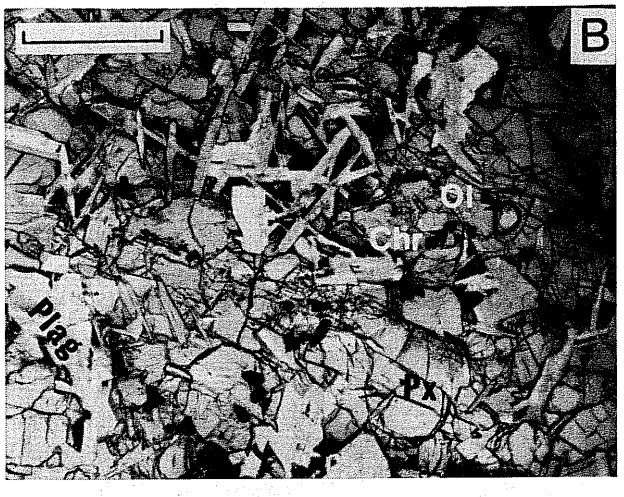

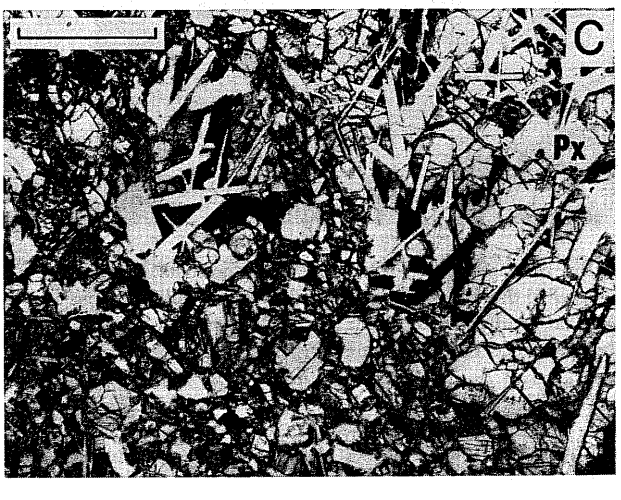

Fig. 2. Three photomicrographs of the HA basalts. The scale bar represents 0.5 mm: **(a)** 14321,1612 illustrating the ophitic basalts; **(b)** 14321,1596 illustrating the subophitic basalts; **(c)** 14321,1594 illustrating the granulated basalts.

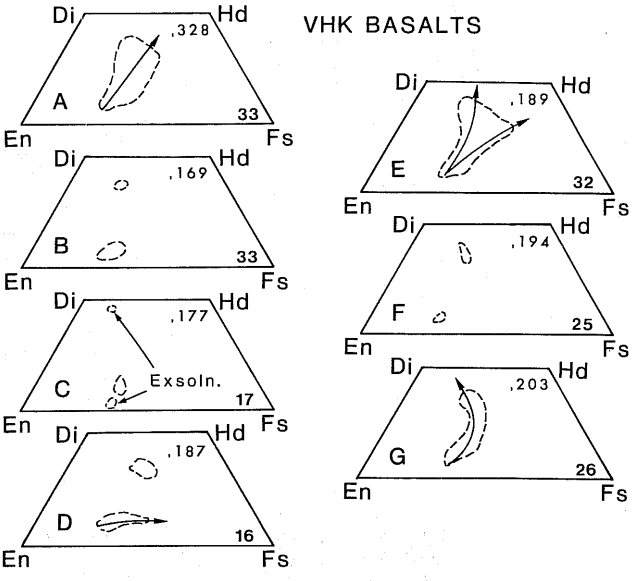

Fig. 3. Pyroxene compositions for each VHK basalt, represented on individual pyroxene quadrilaterals. Numbers refer to the number of analyses and arrows indicate direction of zoning.

Generally, zoning is from Mg-rich (≈En63) cores to Ca- and Fe-rich (≈Wo30; Fs35) rims. In 14304,177(176), one pyroxene exhibits a wormy exsolution texture. The host composition approaches enstatite (En64; Wo2), whereas the composition of the exsolution blebs is close to salite (En42; Wo46) (Fig. 3c). In each VHK basalt, the Al/Ti ratio decreases from the Mg-rich pyroxene cores to the Ca- and Fe-rich rims.

Two types of feldspar are present in the VHK basalts (Table 2), allowing a mineralogical distinction between HA and VHK basalt varieties. The first is an An-rich plagioclase (An81-95; Ab5-17; Fig. 4), exhibiting core-rim zoning toward more Na- and K-rich compositions. The second is K-feldspar (An5-8; Or89-94; Fig. 4), which forms the petrographically unidentifiable overgrowths present on plagioclase crystals (see previous section). Residual K-rich glass (Fig. 4) contains 7-12 wt.% K_2O

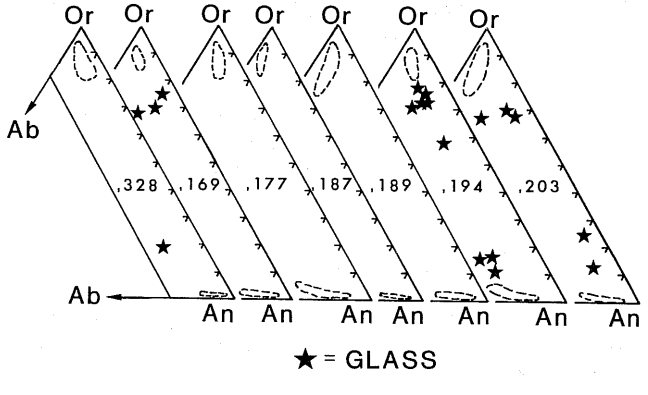

Fig. 4. Potassium-feldspar, plagioclase, and glass compositions for each VHK basalt, represented on individual Or-An-Ab feldspar ternaries.

TABLE 2. Sample numbers and mineral compositions of analyzed VHK basalts.

		14303	14304	14304	14304	14304	14304	14304
PM No.		328	169	177	187	189	194	203
INAA No.		318	168	176	148	152	164	180
Ol	Lo Fo	43-50	—	—	33-37	45-50	46-52	41-46
	Hi Fo	64-65	—	—	56-67	—	—	51-69
	En	31-64	41-67	41-64	32-64	27-63	36-66	31-64
Px	Wo	8-38	4-38	2-46	8-39	8-42	6-40	9-39
	Fs	23-40	19-36	13-36	24-43	19-45	21-28	23-40
	An	90-95	85-96	73-85	88-94	83-93	73-86	81-94
Plag	Ab	4-9	4-13	14-24	5-11	7-15	13-21	5-16
	Or	0-1	0-4	0-3	0-1	0-1	1-6	0-3
	An	1-67	3-75	2-9	1-16	2-75	2-73	1-79
Kspar/	Ab	5-14	6-17	4-33	7-18	5-19	6-22	5-19
Glass	Or	19-94	11-91	81-92	66-92	7-93	5-91	12-94
Ilm	MG#	9-19	—	—	—	8-19	10-15	9-11
Chr	Cr#	60-72	—	—	56-62	76-77	—	57-72
	MG#	7-26	—	—	18-22	13-14	—	10-23
Metal	Ni	0.0-0.5	0.0-4.8	0.0-1.7	0.0-0.9	0.0-0.4	0.0-0.1	0.0-1.1
	Co	0.0-0.1	0.0-0.9	0.0-0.5	0.0-0.2	0.0-0.1	0.0-0.1	0.0-0.5

Cr# = 100[Cr/(Cr+Al)]; MG# = 100[Mg/(Mg+Fe)].

(Table 3). It is silica rich (57-75 wt.% SiO_2; Table 3) accompanied by high alumina (13-22 wt.% Al_2O_3). Barium contents are usually significant in both the K-feldspars and residual glass (≈0.2-4.0 wt.% BaO). These residual glass is low in FeO and TiO_2, and Na_2O is ≈1 wt.%.

Olivine is present in five of the seven new VHK basalts (Table 2). As in other VHK basalts, three of our samples contain both relatively Fo- and Fa-rich olivines (≈Fo65 and ≈Fo40, respectively; Table 2), although olivine compositions in 14304,203(180) may be considered to be continuous. Forsterite-rich olivines exhibit core to rim zoning from ≈Fo69 to ≈Fo55. Generally, the Fa-rich olivines are euhedral and the Fo-rich variants subhedral to anhedral. Two samples contain only one olivine population, ranging approximately from Fo45-52.

Where present, ilmenite is homogeneous within a given grain, but exhibits intergrain variation within a sample. It is always interstitial and associated with residual glass. Chromite in olivine is relatively homogeneous, but when included in pyroxene, it exhibits zoning toward ulvöspinel (Table 2). The Co and Ni contents of FeNi metals (Table 2) reach ≈0.9 wt.% and ≈4.8 wt.%, respectively. Metal compositions from the VHK basalts overlap with metals from "most lunar polymict rocks" of *Ryder et al.* (1980). We do not consider this observation to represent meteorite contamination, as Ir and Au abundances in the whole-rock VHK-basalt chemistry are below detection limits (*Neal et al.*, 1989).

HA Basalts

The new Apollo 14 HA basalts are mineralogically similar to those described by *Dickinson et al.* (1985), *Shervais et al.* (1985a), and *Neal et al.* (1988a). Pyroxenes exhibit a wide range of compositions (Table 4), although little difference is noted between the three textural groups. Figure 5 illustrates the range of pyroxene zoning exhibited by six of the HA basalts. Most are zoned from Mg-rich (En60-64;Wo3-11) cores to more Ca-and Fe-rich (Wo14-23;Fs52-68) rims. Two

TABLE 3. Representative K-rich glass analyses from the VHK basalts.

	14303 ,328	14304 ,169	14304 ,177	14304 ,187	14304 ,189	14304 ,194	14304 ,203
SiO_2	64.4	57.3	71.6	75.5	68.9	59.0	73.5
TiO_2	0.50	0.31	1.40	0.79	1.15	0.29	0.58
Al_2O_3	15.5	22.5	13.2	13.1	15.1	21.1	12.4
Cr_2O_3	0.05	<0.03	<0.03	0.06	<0.03	<0.03	0.04
FeO	1.52	0.41	1.38	0.78	0.73	0.30	1.60
MnO	0.04	<0.03	<0.03	0.04	<0.03	<0.03	0.08
MgO	1.56	0.04	0.10	0.03	0.07	<0.03	0.88
CaO	2.64	3.69	0.42	0.62	0.56	2.39	1.86
BaO	0.21	4.01	0.21	<0.02	0.21	3.23	<0.03
Na_2O	0.49	1.07	0.42	1.43	0.57	0.98	1.31
K_2O	12.3	10.8	10.8	7.32	12.2	12.3	7.00
P_2O_5	0.12	0.16	0.22	0.18	<0.03	<0.03	0.18
TOTAL	99.33	100.29	99.53	99.85	99.49	99.59	99.43

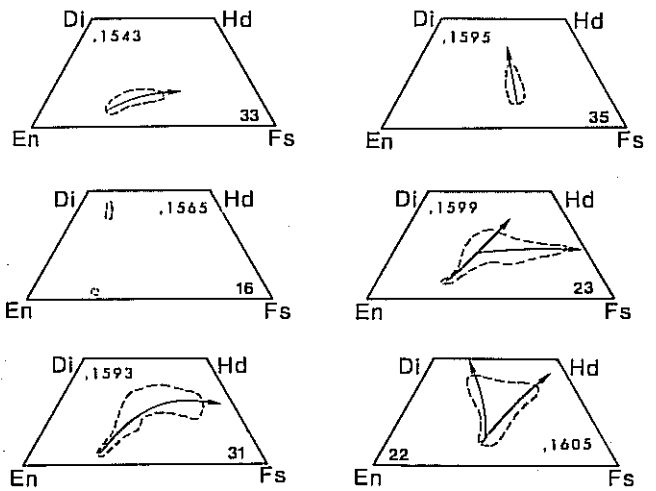

Fig. 5. Pyroxene compositions for each HA basalt, represented on individual pyroxene quadrilaterals. Numbers refer to the number of analyses and arrows indicate direction of zoning.

exceptions from this general trend are (1) pyroxenes from 14321,1565, which exhibit little zoning, and have two types—Mg-rich and Ca-rich, and (2) pyroxenes in 14321,1595(1530) are zoned toward more Ca-rich, Fe-poor compositions (i.e., from En60; Wo7 to En45; Wo30). Generally, Al/Ti ratios are lower in Fe- and Ca-rich pyroxenes.

Plagioclase shows little compositional variation between the three textural groups (Table 4). All exhibit zoning from An-rich (An91-97) cores to more Ab-rich (10-23) and Or-rich (2-4) rims. Iron oxide also shows distinct increases to over 1 wt.% in the rims. Care was taken in the execution of rim analyses such that adjacent grains were not excited.

Olivine is present in all but three basalts studied, compositions varying slightly between the three textural groups (Table 4). The subophitic basalts contain olivines ranging from Fo45-70, whereas the ophitic basalts contain olivines ranging from Fo55-75 (Table 4). Olivines from the granular basalts span the range of the other two groups (Fo45-80).

Chromites are not present in all basalts studied here (see Table 4). Euhedral chromites in olivines are relatively homogeneous, whereas those in pyroxene are subhedral, typically with an increase of TiO_2 and FeO, and a decrease of Al_2O_3 from core to rim. No differences in chromite composition are seen between the three petrographic groups.

Ilmenite is present in all analyzed basalts (Table 4). It is always interstitial and associated with glass, FeNi metal, and troilite. Individual grains are usually homogeneous, but variation between grains in a given sample was noted (Table 4). The residual glass compositions are less silica-rich than in the VHK basalts (45-50 wt.% SiO_2), but are more Ca- and Fe-rich. However, the most distinctive feature of the residual HA basalt glass is the low K_2O contents (<1 wt.%). Iron-nickel metal and troilite grains are also interstitial. Although FeNi metal is present, no analyses were possible from ,1565; ,1595; ,1607; or ,1608. Compositions can vary widely within and between samples (Table 4) and only mildly overlap with metals from "most lunar polymict rocks" of *Ryder et al.* (1980). The Ir and Au abundances in the whole-rock chemistry are below detection limits (*Neal et al.,* 1989), consistent with a lack of meteorite contamination.

PARAGENESIS

VHK Basalts

Very high potassium basalts display a variety of textures. These range from vitrophyric basalts to equigranular, coarse-

TABLE 4. Numbers, texture, and mineral compositions within analyzed HA basalts.

Sample	Texture	Ol	Plag		Pyroxene		Chromite		Ilm	Metal	
PM/INAA		Fo	An	Ab	Wo	En	Cr#	Mg#	Mg#	Ni	Co
1543/----	SO	61-65	76-91	8-21	7-16	52-64	55-57	21-24	2-7	0.2-1.3	0.2-1.6
1565/----	G	67-70	82-95	4-14	3-44	44-71	—		19-26	—	—
1591/1520	G	48-50	75-95	4-14	8-38	8-15	56-60	32-34	11-12	0.3-0.5	0.1-0.2
1592/1522	G	77-80	77-94	6-21	8-35	14-63	54-60	13-23	1-4	0.0-1.7	0.0-0.9
1593/1524	SO	51-59	80-96	3-18	7-36	14-65	—		2-11	1.9-3.2	0.0-2.6
1594/1529	G	50-55	81-94	6-17	8-31	15-62	56-59	19-21	2-12	0.7-3.1	0.0-2.6
1595/1530	SO	45-49	88-96	4-11	13-29	33-40	—		11-12	—	—
1596/1533	SO	—	85-93	7-14	8-15	26-64	55-59	27-30	4-9	0.1-0.6	0.1-0.2
1597/1535	SO	61-64	87-96	4-10	8-30	36-63	54-64	16-20	4-11	0.5-12.3	0.0-4.4
1598/1538	O	58-61	77-93	7-21	10-36	14-56	—		1-12	0.0-0.1	0.0-0.4
1599/1546	G	51-62	81-93	7-17	8-31	10-65	54-64	14-26	1-10	0.2-3.3	0.0-0.2
1600/1563	SO	65-67	77-94	6-20	8-27	20-63	—		3-6	0.0-11.1	0.0-1.7
1601/1518	G	—	75-93	6-23	9-35	12-64	70-71	9-10	9-11	0.9-2.7	0.2-0.3
1604/1549	G	51-65	83-96	4-16	8-33	23-63	57-66	15-21	4-13	0.0-0.2	0.1-0.2
1605/1553	O	60-75	79-97	2-19	10-31	23-50	54-58	22-30	5-17	0.1-4.4	0.1-1.2
1606/1556	O	63-72	78-93	7-19	9-37	7-53	50-59	17-27	1-9	0.0-0.1	0.0-0.1
1607/1558	G	50-63	81-94	6-17	7-28	13-65	58-69	14-18	11-14	—	—
1608/1568	O	57-63	83-96	4-15	8-36	14-63	—		3-12	—	—
1609/1573	O	61-73	76-92	8-21	10-37	22-59	58-66	19-28	1-9	0.0-12.7	0.0-2.3
1610/1578	G	49-56	78-97	3-20	12-29	7-58	54-68	11-21	3-12	3.0-9.5	0.6-2.7
1611/1582	G	—	88-95	5-11	9-26	10-63	54-59	17-28	4-16	0.3-3.4	0.0-0.3
1612/1585	O	59-68	82-93	7-16	12-38	10-53	47-58	21-28	1-11	0.0-0.2	0.0-0.2

SO = subophitic; O = ophitic; G = granulated; Cr# = 100 [Cr/(Cr+Al)]; Mg# = 100 [Mg/(Mg + Fe)].

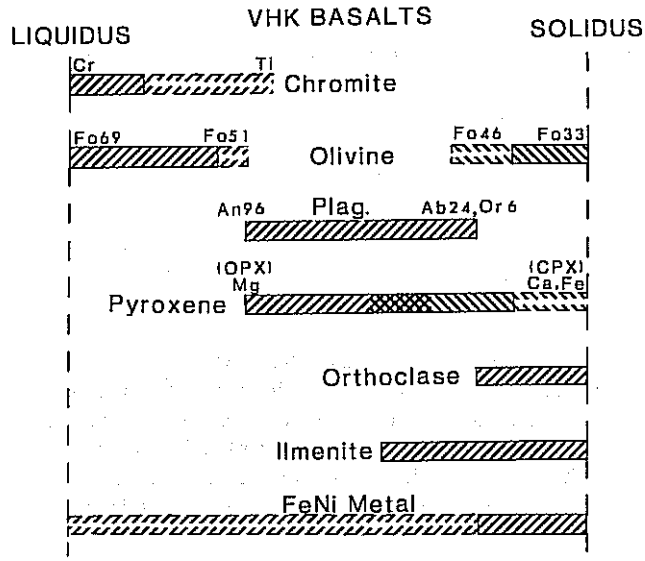

Fig. 6. Crystallization sequence deduced for the VHK basalts. Fields with dashed outlines and a median break indicate that this phase is only on the liquidus in some samples at this point. The field for FeNi metal also includes that for troilite. The chemistry included on this diagram is designed to demonstrate the zoning of minerals as well as absolute ranges. The ornamentation for the pyroxene field illustrates the overlap of Ca- and Fe-rich pyroxenes with Mg-rich varieties.

grained (up to 1.5 mm) types. Plagioclase laths may intrude into, or be terminated by, the pyroxene prisms. Overgrowths of K-feldspar on plagioclase are present in all samples, as is interstitial K-rich glass. Euhedral Fa-rich olivines are present, and three samples also contain subhedral to anhedral Fo-rich olivines with FeNi metal inclusions. Chromites are present as euhedral inclusions in olivine, subhedral inclusions in pyroxene, or as minor interstitial phases. The pyroxene exsolution texture present in 14304,177(,176) indicates a slow-cooling igneous origin, either from the center of large flow or a hypabyssal intrusion.

The petrographic variation suggests the following paragenetic sequence (Fig. 6). Olivine (high-Fo), chromite, and, in some cases, FeNi metal were the first phases to crystallize, followed by pyroxene and plagioclase. High-Mg pyroxene formed reaction rims around and therefore crystallize after olivine. Later pyroxenes were more Ca- and Fe-rich. Petrographic relationships and core to rim zoning of Al/Ti in pyroxene suggest plagioclase cocrystallized with pyroxene (*Bence and Papike,* 1972). Plagioclase exhibits zoning toward more Na- and K-rich compositions. Chromite continued to crystallize after olivine precipitation ceased, as it is included in pyroxene and also forms a minor interstitial phase in some VHK basalts. The early chromites in olivine are relatively homogeneous, as early inclusion in olivine effectively isolates it from the evolving magma. Chromite inclusions in pyroxene and the minor interstitial chromites are zoned towards ulvöspinel compositions. Ilmenite, K-feldspar, Fa-rich olivine, and FeNi metal are identified as late-stage fractionates because: (1) although individual ilmenite grains are homogeneous, there is intergrain variation due to the isolated nature of the residual magma pockets from which they crystallized; (2) K-feldspar forms overgrowths on plagioclase; (3) Fa-rich olivine is euhedral and interstitial; and (4) the interstitial nature of most FeNi metal. These phases were precipitated from the residual melt, which is evidenced in the K-rich residual glass. Such crystallization is responsible for the low Ti and Fe in the residual glass, but it cannot account for the high K_2O content, especially as K-feldspar is precipitating.

HA Basalts

A high-alumina basalt typically contains olivine phenocrysts, with or without a pyroxene reaction rim, set in a network of pyroxene prisms and plagioclase laths. Plagioclase laths may intrude into, or be terminated by, the pyroxene prisms. Overall grain size does not exceed 2 mm. Chromite is found as inclusions in olivine phenocrysts and pyroxene. Ilmenite, SiO_2, FeNi metal, and troilite are interstitial phases, often set in opaque residual glass. The residual HA basalt glass compositions contain significantly lower K_2O (<1 wt.%) than the VHK basalt residual glass and is less silica-rich due to late-stage SiO_2 precipitation.

The petrography and mineral chemistry of the HA basalts suggest the following paragenetic sequence (Fig. 7). Olivine and chromite were the first phases to crystallize, followed by pyroxene and plagioclase. The first pyroxenes to crystallize were generally pigeonites and formed reaction rims around

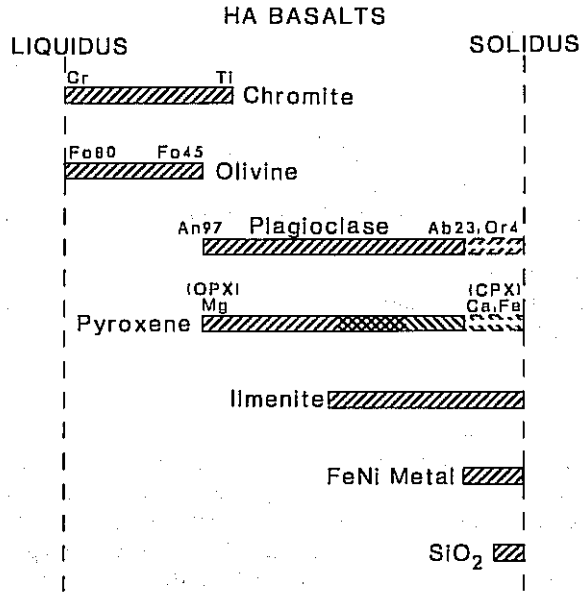

Fig. 7. Crystallization sequence deduced for the HA basalts. Fields with dashed outlines and a median break indicate that this phase is only on the liquidus in some samples at this point. The field for FeNi metal also includes that for troilite. The chemistry included on this diagram is designed to demonstrate the zoning of minerals as well as absolute ranges. The ornamentation for the pyroxene field illustrates the overlap of Ca- and Fe-rich pyroxenes with Mg-rich varieties.

olivine. Later pyroxenes were more Ca- and Fe-rich. Petrographic relationships and core to rim zonings of Al/Ti in pyroxene suggest cocrystallization with plagioclase (*Bence and Papike,* 1972). Plagioclase exhibits zoning toward more Na-and K-rich compositions. Olivine crystallization ceased with the onset of plagioclase and pyroxene crystallization. However, chromite continued to crystallize during pyroxene fractionation. These later chromites are zoned toward ulvöspinel compositions, whereas those in olivine that formed earlier are relatively homogeneous. These relationships indicate that chromites included in pyroxene have experienced continued growth from an evolving magma. Ilmenite, FeNi metal, and SiO_2 were the final crystallization products.

PETROGENESIS

Petrography and mineral chemistry demonstrate that the VHK and HA basalts experienced similar crystallization histories. Petrography is consistent with the whole-rock chemistry (*Neal et al.,* 1988a,b) in that olivine and chromite were the first phases to crystallize. Both magmas evolved to more K, Na, Ca, Fe, and Ti rich compositions. However, there are differences between the two compositions that allow their petrogeneses to be distinguished.

VHK Basalts

The mineralogy of VHK basalts supports this classification of these samples in that extreme potassium enrichment is witnessed by the presence of K-feldspar and residual K-rich glass. The interstitial K-rich glass represents the composition of the residual magma. The abundance of K (7-12 wt.% K_2O) in this residual glass is above what would be expected from fractional crystallization alone and requires some external input of K into the magma. This observation is consistent with the AFC model proposed for the petrogenesis of VHK basalts (*Shervais et al.,* 1985b; *Goodrich et al.,* 1986; *Warren et al.,* 1986; *Neal et al.,* 1988a,b). In these models, a crystallizing HA magma assimilates lunar granite, which imparts the very high potassium signature to these magmas witnessed by the occurrence of K-feldspar and the high K_2O contents of the residual melt.

HA Basalts

The mineralogy and petrography of the HA basalts also gives an indication of their petrogenesis. Although these basalts underwent K enrichment during fractionation, abundances were not sufficient to cause K-feldspar crystallization (i.e., <1 wt.% K_2O in the residual melt). The mineral zoning and petrographic relationships observed in the HA basalts are consistent with a basaltic magma undergoing normal fractional crystallization. However, based on whole-rock trace-element chemistry, *Neal et al.* (1988b; *Neal et al.*, 1989) proposed an AFC model involving the assimilation of KREEP by a parental magma to account for HA basalt petrogenesis. This is not apparent from the mineralogy and petrography of these basalts, although those with "primitive" mineralogies (i.e., large olivine phenocrysts with little or no reaction rims) generally exhibit "primitive" whole-rock trace-element chemistries (e.g., low incompatible element abundances; see *Neal et al.,* 1989). This may be due to the major-element similarities between the KREEP assimilant and a primitive HA basalt (e.g., *Warren and Wasson,* 1979; *Vaniman and Papike,* 1980).

CONCLUSIONS

The above study outlines the evolution of VHK and HA basalts as determined from mineralogy and petrography. Crystallization sequences are generally similar for both VHK and HA basalts, with mineralogical differences occurring in the late stages of crystallization. Both texture and mineral zoning indicate that the parental magmas had sufficient time to evolve and generate reasonably coarse grain sizes. The VHK and HA parental magmas became enriched in Fe, Ti (culminating in late-stage ilmenite), Na, and K, and depleted in Mg and Al as crystallization proceeded. However, the composition of the residual magma in VHK basalts contains K abundances over and above that that could be produced by fractional crystallization alone, resulting in K-feldspar crystallization. Therefore an external source of K is required. This is consistent with the model of granite assimilation developed by consideration of the whole-rock compositions.

The mineralogy and petrography suggests HA basalts evolved by fractional crystallization alone, with little evidence for KREEP involvement. In this instance, it is the whole-rock chemistry that is the essential data for determining HA basalt petrogenesis. As such, this study of HA basalts emphasizes that the correct approach to petrology is a combination of mineralogy and petrography with whole-rock major- and trace-element chemistry.

Acknowledgments. This work would not have been possible without the capable assistance of the Curatorial Staff in the Planetary Materials Branch at NASA Johnson Space Center. Thoughtful reviews by D. Lindstrom, B. Schuraytz, J. Taylor, and G. Ryder were greatly appreciated. The Cameca electron microprobe was purchased with funds from NASA and NSF through grants to L. A. Taylor. This research was supported by NASA grant NAG 9-62 to L. A. Taylor.

REFERENCES

Bence A. E. and Papike J. J. (1972) Pyroxenes as recorders of lunar basalt petrogenesis: Chemical trends due to crystal-liquid interactions. *Proc. Lunar Sci. Conf. 3rd,* pp. 431-469.

Dickinson T., Taylor G. J., Keil K., Schmitt R. A., Hughes S. S., and Smith M. R. (1985) Apollo 14 aluminous mare basalts and their possible relationship to KREEP. *Proc. Lunar Planet. Sci. Conf. 15th* in *J. Geophys. Res., 90,* C365-C374.

Goodrich C. A., Taylor G. J., Keil K., Kallemeyn G. W., and Warren P. H. (1986) Alkali norite, troctolites, and VHK mare basalts from breccia 14304. *Proc. Lunar Planet. Sci. Conf. 16th,* in *J. Geophys. Res., 91,* D305-D318.

Neal C. R., Taylor L. A., and Lindstrom M. M. (1988a) The importance of lunar granite and KREEP in Very High Potassium (VHK) basalt petrogenesis. *Proc. Lunar Planet. Sci. Conf. 18th,* pp. 121-137.

Neal C. R., Taylor L. A., and Lindstrom M. M. (1988b) Apollo 14 mare basalt petrogenesis: Assimilation of KREEP-like components by a fractionating magma. *Proc. Lunar Planet. Sci. Conf. 18th,* pp. 139-153.

Neal C. R., Taylor L. A., Patchen A. D., Schmitt R. A., Hughes S. S., and Lindstrom M. M. (1989) HA and VHK basalt clasts from Apollo 14

breccias: Part 2—whole rock geochemistry. Further evidence for combined assimilation and fractional crystallization within the lunar crust. *Proc. Lunar Planet. Sci. Conf. 19th,* this volume.

Ryder G., Norman M. D., and Score R. A. (1980) The distinction of pristine from meteorite-contaminated highland rocks using metal compositions. *Proc. Lunar Planet. Sci. Conf. 11th,* pp. 471–480.

Shervais J. W., Taylor L. A., and Lindstrom M. M. (1985a) Apollo 14 mare basalts: Petrology and geochemistry of clasts from consortium breccia 14321. *Proc. Lunar Planet. Sci. Conf. 15th,* in *J. Geophys. Res., 90,* C375–C395.

Shervais J. W., Taylor L. A., Laul J. C., Shih C.-Y., and Nyquist L. E. (1985b) Very high potassium (VHK) basalt: Complications in Mare Basalt petrogenesis. *Proc. Lunar Planet. Sci. Conf. 16th,* in *J. Geophys. Res., 90,* D3–D18.

Vaniman D. T. and Papike J. J. (1980) Lunar highland melt rocks: Chemistry, petrology, and silicate mineralogy. In *Proceedings of the Conference on the Lunar Highlands Crust* (J. J. Papike and R. B. Merrill, eds.), pp. 271–337. Pergamon, New York.

Warren P. H. and Wasson J. T. (1979) The origin of KREEP. *Rev. Geophys. Space Phys., 17,* 73–88.

Warren P. H., Shirley D. N., and Kallemeyn G. W. (1986) A potpourri of pristine moon rocks, including a VHK mare basalt and a unique, Augite-rich Apollo 17 anorthosite. *Proc. Lunar Planet. Sci. Conf. 16th,* in *J. Geophys. Res., 91,* D319–D330.